# Slow crack growth in multispectral zinc sulfide for use in aircraft window design

**Colin M. Ryan,[a,*] Daniel C. Harris,[a] Jared C. Wright,[b] Ashlynn M. Stanley,[b] and Sung R. Choi[b]**

[a]Naval Air Warfare Center Weapons Division, China Lake, California, United States
[b]Naval Air Warfare Center Aircraft Division, Patuxent River, Maryland, United States

**Abstract.** The slow crack growth rate and inert strength of multispectral zinc sulfide were measured for use in aircraft window lifetime analysis. Dynamic fatigue data for uncoated multispectral zinc sulfide were fit to a power law by linear regression and to an exponential law by computer-aided numerical integration to obtain best-fit slow crack growth rate parameters. For the power law slow crack growth equation, crack velocity $(v) = A^*(K_I/K_{Ic})^n$, we find $A^* = 0.00769$ m/s and $n = 14.65$, where $K_I$ is the stress intensity factor, $K_{Ic} = 0.72$ MPa$\sqrt{\text{m}}$ is the critical stress intensity factor, and we assign the value of the geometric factor to be $Y = 2/\sqrt{\pi}$. Parameters for the exponential law slow crack growth equation, crack velocity $(v) = v_o \exp(\beta K_I)$ are $v_o = 3.02 \times 10^{-14}$ m/s and $\beta = 43.64$ (MPa$\sqrt{\text{m}}$)$^{-1}$. There were only small differences in the crack growth rate between uncoated and antireflection-coated material. The crack growth rate that we observe is 10 to 200 times faster than previously reported for a stress intensity factor $K_I = 0.25$ MPa$\sqrt{\text{m}}$, which is a representative value of $K_I$ for an aircraft window in service. The faster crack growth rate predicts a correspondingly shorter window lifetime. The inert strength of uncoated biaxial flexure disks (38.1 mm diameter with 15.88 mm load diameter and 31.75 mm support diameter) measured in dry nitrogen exhibited a 50% Weibull failure probability at 115 MPa with an unbiased ASTM C1239 Weibull modulus of 4.68. Antireflection-coated material had a 50% Weibull failure probability at 100 MPa with a Weibull modulus of 5.25.  [DOI: 10.1117/1.OE.61.4.047103]

**Keywords:** multispectral zinc sulfide; zinc sulfide; slow crack growth; optical window design; dynamic fatigue; exponential crack growth law.

Paper 20220019G received Jan. 5, 2022; accepted for publication Mar. 2, 2022; published online Apr. 14, 2022.

## 1 Background

Multispectral zinc sulfide (MS-ZnS), also known as Cleartran® or Waterclear® zinc sulfide, is a polycrystalline ceramic window material with transparency from visible through mid-wave (3 to 5 $\mu$m) to long-wave (8 to 12 $\mu$m) infrared wavelengths and a cubic sphalerite crystal structure. It was discovered accidentally by C. B. Willingham at Raytheon Research Division in 1979 when he applied the newly available procedure of hot isostatic pressing to "standard" grade orange-yellow, translucent, chemical-vapor-deposited zinc sulfide, which is only useful in the long-wave infrared region.[1] He was hoping to remove traces of residual porosity and hexagonal phase. To protect the material from oxidation by traces of $O_2$ in the high-pressure argon gas used for hot isostatic pressing, Willingham wrapped his samples in platinum foil. When he unwrapped the zinc sulfide after hot isostatic pressing, he was amazed to observe that the translucent colored material had been transformed into clear, colorless material now called multispectral zinc sulfide. It was later learned that platinum foil is essential to the chemistry that transforms yellow-orange zinc sulfide into clear, colorless zinc sulfide. If he had not wrapped the sample in platinum foil, MS-ZnS might never have been discovered.

MS-ZnS is a relatively soft ceramic with modest mechanical strength. It is easily damaged by sand abrasion or rain impact at aircraft speeds. In our application for MS-ZnS as an infrared

*Address all correspondence to Colin Ryan, colin.m.ryan2.civ@us.navy.mil

sensor window for an airplane, the external surface of the window is in tension when the cabin pressure is greater than the external atmospheric pressure. In the absence of surface damage, the window lifetime is expected to be limited by the rate at which microscopic cracks in the material propagate to failure under the influence of tensile stress.

We are aware of one previous measurement of the slow crack growth rate in MS-ZnS (Cleartran® from Morton International, Weeks Island, Louisiana, United States) in 1993.[2,3] Our MS-ZnS was manufactured by II-VI, Inc. (Saxonburg, Pennsylvania, United States). To characterize our window material, we measured the slow crack growth in coupons of II-VI MS-ZnS taken from the same two blank plates from which two aircraft windows were manufactured.

## 2 Slow Crack Growth

When a flaw in a brittle material is subject to tensile stress in a reactive environment, bonds at the tip of the flaw can be chemically attacked and broken, resulting in the growth of the flaw.[4,5] For many materials including MS-ZnS, water, and, by extension, atmospheric humidity promote crack extension. The strength of a material measured in the absence of slow crack growth is called the inert strength ($\sigma_i$). When measured in a reactive environment, slow crack growth occurs during the application of stress, so the failure stress ($\sigma_f$) is less than the inert strength. For conservative window design, the slow crack growth rate is usually measured with test coupons immersed in liquid water to obtain an overestimate of crack growth rate in ambient humidity in the air.

The most common method for measuring the slow crack growth rate is dynamic fatigue. Test coupons are exposed to a series of constantly applied stress rates $\dot{\sigma}_a = d\sigma_a/dt$ while submerged in water ($\sigma_a$ is applied stress and $t$ is time). The lower the stress rate is, the more time is needed to reach failure stress and the lower the failure strength is due to slow crack growth during the test. At high-stress rates, there is less time for slow crack growth to occur, so the failure stress is greater.

The slow crack growth rate ($v$) is generally described using two types of empirical equations:

1. The exponential law is given by

$$v = \frac{dc}{dt} = v_o e^{\beta K_I}, \tag{1}$$

   where $c$ is flaw size, $t$ is time, $v_o$ and $\beta$ are measured parameters, and $K_I$ is the stress intensity factor, which is proportional to the magnitude of the stress field at the crack tip and

2. The power law is given by

$$v = \frac{dc}{dt} = A^* \left(\frac{K_I}{K_{Ic}}\right)^n, \tag{2}$$

   where $A^*$ and $n$ are measured parameters and $K_{Ic}$ is the critical stress intensity factor for catastrophic failure.

ASTM C1368 and C1465 describe the use of dynamic fatigue testing to determine power law parameters $A^*$ and $n$.[6,7] For a constant applied stress rate $\dot{\sigma}_a$, the power law provides a relation of failure strength ($\sigma_f$) to stress rate ($\dot{\sigma}_a$) and inert strength ($\sigma_i$) through Eq. (3), which is given as

$$\sigma_f^{n+1} = \frac{2K_{Ic}^2}{A^* Y^2 (n-2)} (n+1) \sigma_i^{n-2} \dot{\sigma}_a, \tag{3}$$

where $Y$ is a geometric factor, which in this work is taken as $Y = 2/\sqrt{\pi}$ for a halfpenny flaw, and $\sigma_i$ is taken in our work as the 50% Weibull failure probability for samples tested in an inert environment.

Taking the logarithm of both sides of Eq. (3) produces a useful equation:

$$\log(\sigma_f) = \left(\frac{1}{n+1}\right) \log(\dot{\sigma}_a) + \left(\frac{1}{n+1}\right) \log\left(\frac{2K_{Ic}^2}{A^* Y^2 (n-2)} [n+1] \sigma_i^{n-2}\right). \tag{4}$$

According to Eq. (4), the relationship between $\log(\sigma_f)$ and $\log(\dot{\sigma}_a)$ should be linear. We use linear regression to find the best-fit slope ($a$) and intercept ($b$). Crack growth parameters $n$ and $A^*$ in Eq. (2) are then found from the following relations, which are stated as

$$n = \frac{1}{a} - 1, \tag{5}$$

$$A^* = \frac{2K_{Ic}^2 \sigma_i^{\left(\frac{1}{a} - 3\right)}}{a(10^{b/a}) Y^2 (n-2)}. \tag{6}$$

By contrast, the exponential law Eq. (1) does not have an analytical solution for the failure strength. However, Eq. (1) can be numerically integrated to calculate $\sigma_f$ for each experimental value of $\dot{\sigma}_a$ and trial values of parameters $v_o$ and $\beta$ in Eq. (1). In a separate paper, we describe a numerical integration procedure using an optimization algorithm to find the values of $v_o$ and $\beta$ that minimize the sum of squares of differences between calculated values of $\log(\sigma_f)$ and observed values of $\log(\sigma_f)$ for each experimental value of $\dot{\sigma}_a$.[8]

A window material might follow the exponential law Eq. (1) or the power law Eq. (2) over a wide range of stress intensity factors $K_I$. However, it is difficult to measure slow crack growth down to the low values of $K_I$ that apply to most of the service life of a window. In the absence of knowing whether the exponential law or the power law better represents the behavior of a given window material, the U.S. National Aeronautics and Space Administration prescribes that the more conservative exponential law be used to predict the service life.[9] The window lifetime predicted by the exponential law can be one or more orders of magnitude less than the lifetime predicted by the power law fit to the same dynamic fatigue measurements.

## 3 Experimental

### 3.1 *Materials and Test Specimens*

Two multispectral zinc sulfide plates were produced by II-VI Inc. (Saxonburg, Pennsylvania, United States), and test specimens were fabricated from the plates by II-VI Aerospace & Defense (Murrieta, California, United States). For sets of 30 coupons in each flexure test condition, 15 were taken from each of the two MS-ZnS blank plates. Test specimens were randomized to minimize systematic errors associated with their orientations and locations in the blank plate. Disks for inert strength and dynamic fatigue testing had a nominal diameter of 38.1 mm and thickness of 2.00 mm with chamfered edges. Both faces had a 60/40 scratch/dig (MIL-PRF-13830B) optical polish. Some disks had a proprietary antireflection coating on both faces. Fracture toughness was measured on #600 grit ground flexure beams with dimensions 5.0 mm × 8.0 mm × 45 mm representing width, depth, and length, respectively.

### 3.2 *Inert Strength*

Inert strength was determined by biaxial flexure of 30 disks with a load diameter of 15.88 mm and support diameter of 31.75 mm in dry nitrogen with a stress rate of 10 MPa/s under load control using an electromechanical test frame (Model 5982, Instron, Norwood, Massachusetts, United States). A ring-shaped Teflon sheet with a thickness of 20 $\mu$m was placed between the disk and the load and support rings to reduce friction. Adhesive tape was applied to the compressive surface of the disk to retain fragments. For drying, disks were placed in slots in an acrylic fixture in a bell jar and evacuated overnight. Ultrahigh purity nitrogen containing ~2 ppm water was admitted to the bell jar, and one disk was taken out in the air and placed in the flexure test fixture. The remaining disks were evacuated again. The flexure test fixture was preloaded to 10 N with dry nitrogen flowing over the tensile face for >3 min before beginning the tensile test with nitrogen continuing to flow.

### 3.3 *Slow Crack Growth (Dynamic Fatigue)*

Dynamic fatigue testing was carried out in biaxial flexure at room temperature in distilled water in accordance with ASTM C1368.[6] The test fixture, test frame, and dimensions of test specimens used in dynamic fatigue testing were the same as those in inert strength testing. Five different nominal applied stress rates of 10, 1, 0.1, 0.01, and 0.001 MPa/s were employed. For the lowest stress rate of 0.001 MPa/s, disks were preloaded at 20% to 50% of the expected failure stress to reduce the time required for these long tests.[6,10,11] Thirty test specimens were used at each test rate for statistical reproducibility and repeatability of design data.[12,13] Test specimens were randomized to minimize possible systematic errors associated with their locations in the blank plate.

Failure strength ($\sigma_f$) of test specimens subject to biaxial flexure was calculated based on the following equation,[14] which applies inside the load radius and is given by

$$\sigma_f = \frac{3F(1-\nu)}{4\pi d^2}\left(\frac{r_s^2 - r_l^2}{r_d^2} - 2\frac{1+\nu}{1-\nu}\ln\frac{r_l}{r_s}\right), \tag{7}$$

where $r_l$ is the load radius, $r_s$ is the support radius, $r_d$ is the test specimen (disk) radius, $d$ is the disk thickness, $F$ is the fracture force, and $\nu$ is Poisson's ratio of MS-ZnS. The thickness of each test specimen was measured after the test and used in Eq. (7).

### 3.4 *Fracture Toughness*

Fracture toughness[15] was determined on dry coupons in an atmosphere of ultrahigh purity $N_2$ using the single edge V-notched beam (SEVNB) method.[16,17] The V-notch plane was perpendicular to the 5 mm × 45 mm face of each flexure bar. A sharp razor blade with 1 $\mu$m diamond abrasive was placed into a straight saw-notch precut at the middle of a flexure test specimen to cut a sharp V-notch with its root radius typically <10 to 20 $\mu$m (Fig. 1). The ratio of sharp-notch length to test-specimen depth was in the range of 0.2 to 0.3. Fracture toughness was measured with a four-point flexure fixture with 20 mm-inner and 40 mm-outer spans. Test specimens with a length of 22 mm (instead of 45 mm) were measured by three-point flexure with a support span of 20 mm. A test rate of 0.2 mm/ min was applied to test specimens via the same test frame used for inert strength and dynamic fatigue testing. The sharp-notch length was measured with a digital microscope (Model VHX-S750E, Keyence, Japan) from the fracture surface of each broken test specimen based on a three-point measurement per ASTM C1421. Eleven test specimens were used in fracture toughness testing. Fracture toughness was calculated based on the formulas given in ASTM C1421.

### 3.5 *Elastic Modulus*

Elastic modulus was determined at ambient temperature by impulse excitation with a Grindosonic MK-7 (Belgium) in accordance with ASTM C1259.[18] By inducing combined flexural and torsional excitations/vibrations by a miniature soft exciter ("hammer") in a disk, the elastic (Young's) modulus $E$, shear modulus ($G$), and Poisson's ratio ($\nu$) are obtained through

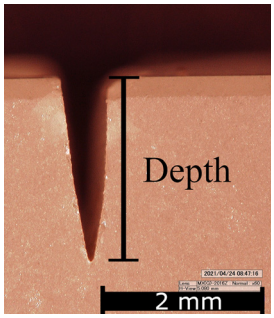


**Fig. 1** V-notch generated on a flexure specimen for measuring fracture toughness (notch root radius ~ 20 $\mu$m). The marker bar is 2 mm.

the iteration/convergence procedure described in ASTM C1259. The procedure is incorporated in conjunction with the relationship $G = E/[2(1+\nu)]$. Twenty-eight coupons including 18 uncoated disks and 10 flexure bars were used to measure $E$ and density. Eighteen disks were used for $E$, $G$, and $\nu$. Density was determined by measuring the mass and volume for the 28 coupons and input to the elastic modulus measurements.

### 3.6 *Microhardness*

Vickers microhardness was determined in accordance with ASTM C1327.[19] Four different indent forces ranging from 0.98 to 9.81 N were employed with a total of 10 measurements at each indent force via a Vickers microhardness tester (Model Tukon 2100B, Wilson–Wolpert, Instron, Canton, Massachusetts, United States). The samples used in microhardness testing were broken fragments of uncoated disks after their inert strength testing.

## 4 Results

Table 1 summarizes measured values of elastic constants, hardness, and density.

### 4.1 *Inert Strength Weibull Parameters*

All disks for inert strength and dynamic fatigue failed within the load ring diameter at surface or subsurface damage associated with processing or from surface/subsurface grains. Figure 2 shows Weibull plots for the inert strength of uncoated and antireflection-coated MS-ZnS in dry nitrogen. The maximum likelihood method in ASTM C1239[23] was used to compute Weibull parameters in Table 2.

Curves in Fig. 2 were fit to the Weibull equation

$$P_f = 1 - e^{-\left(\frac{\sigma}{\sigma_\theta}\right)^m}, \tag{8}$$

where $P_f$ is the probability of failure, $\sigma$ is the applied stress, $\sigma_\theta$ is the characteristic strength, and $m$ is the Weibull modulus. The form of the Weibull equation that allows for area scaling is

$$P_f = 1 - e^{-\left(\frac{A_e}{A_o}\right)\left(\frac{\sigma}{\sigma_o}\right)^m}, \tag{9}$$

**Table 1** Elastic constants, microhardness, and density of MS-ZnS.

| Type of test | Test method | No. of test specimens | Measured value[a] | Literature values |
|---|---|---|---|---|
| Fracture toughness $K_{Ic}$ (MPa$\sqrt{m}$) | SEVNB[16,17] (ASTM C1421) | 11 | 0.72 (0.08) | 0.74 (0.14)[b] |
| Young's modulus $E$ (GPa), shear modulus $G$ (GPa), Poisson's ratio $\nu$ | Impulse excitation of vibration (ASTM C1259) | 18 to 28 | $E = 90.0$ (1.09), $G = 33.3$ (0.61), $\nu = 0.35$ (0.01) | $E = 91$[b], 88[c], and 89[d], $\nu = 0.32$[c] and 0.33[d] |
| Density $\rho$ (g/cm$^3$) | Mass/volume | 28 | 4.06 (0.01) | 4.090 theoretical for unit cell 0.5409 nm |
| Microhardness $H$ (GPa) | Vickers indentation (ASTM C1327) | 10 measurements per indent force with four indent forces | 1.46 (0.08) | |

[a]Numbers in parentheses are ±1.0 standard deviation.
[b]II-VI MS-ZnS.[20]
[c]Raytheon MS-ZnS.[21]
[d]Rohm and Haas MS-ZnS.[22]

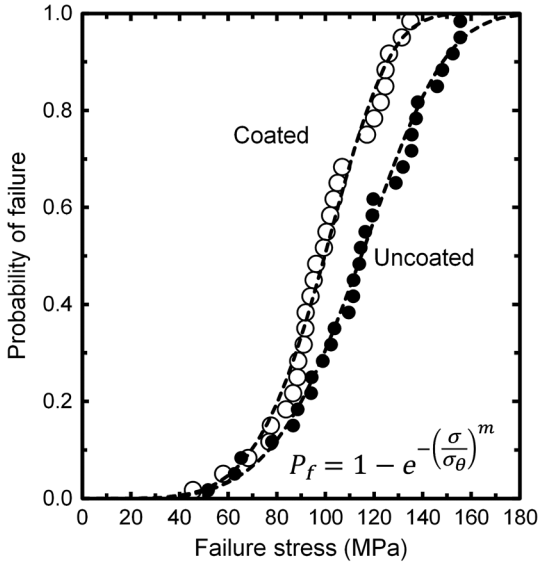


**Fig. 2** Inert strength Weibull distributions for uncoated and antireflection-coated MS-ZnS.

**Table 2** Inert strength Weibull parameters.

| Weibull parameters | Uncoated MS-ZnS | Coated MS-ZnS | Cleartran[2] 1993 data |
|---|---|---|---|
| Weibull modulus $m$ (unbiased) | 4.68 | 5.25 | 5.93 |
| Characteristic strength $\sigma_\theta$ (MPa) | 124.1 | 106.9 | 95.8 |
| Scale factor $\sigma_o$ (MPa) | 181.9 | 149.4 | 121.3 |
| Coupon effective area $A_e$ (cm$^2$) | 6.00 | 5.78 | 4.04 |
| Stress at 50% failure probability | 114.7 | 99.7 | 90.4 |

where $A_e$ is the effective area in tension, $A_o$ is the unit area (1 cm$^2$) for unit cancelation, and $\sigma_o$ is the Weibull scale factor, which is the characteristic strength for a 1 cm$^2$ area in uniaxial tension. The relation between the characteristic strength $\sigma_\theta$ and the Weibull scale factor $\sigma_o$ is

$$\sigma_o = \left(\frac{A_e}{A_o}\right)^{1/m} \sigma_\theta. \tag{10}$$

The effective area $A_e$ for a disk in an equibiaxial flexure test is[24]

$$A_e = 2\pi r_l^2 \left\{1 + \frac{44(1+\nu)}{3(1+\mathrm{m})} \frac{5+\mathrm{m}}{2+\mathrm{m}} \left(\frac{r_s - r_l}{r_s r_d}\right)^2 \left[\frac{2r_d^2(1+\nu) + (r_s - r_l)^2(1-\nu)}{(3+\nu)(1+3\nu)}\right]\right\}, \tag{11}$$

where $\nu$ is Poisson's ratio, $m$ is the Weibull modulus, $r_l$ is the load radius, $r_s$ is the support radius, and $r_d$ is the disk radius.

We display the strength of both uncoated and antireflection-coated material in Fig. 2 because there are few examples in the literature showing the effect of coating on mechanical strength. For both the strength and the rate of slow crack growth (presented in the Sec. 4.2), we find only small differences between coated and uncoated material. This behavior is not unexpected but is rarely investigated.

The mean strength of 30 uncoated disks of MS-ZnS was 113.5 MPa with a standard deviation of 27.9 MPa. The mean strength of 30 coated disks was 98.7 ± 21.3 MPa. The coated disks are 87% as strong as the uncoated disks for this particular anti-reflection coating. The difference in

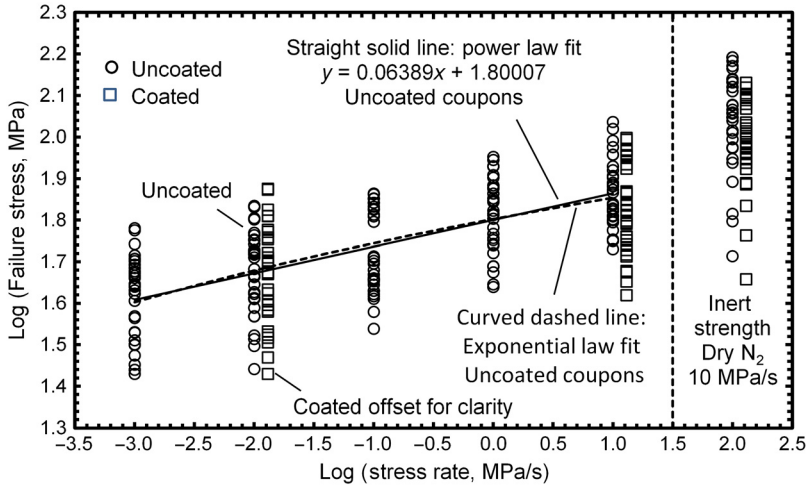


**Fig. 3** Dynamic fatigue measurements of optically polished MS-ZnS disks in distilled water at 21.8°C to 24.6°C. Round points are uncoated samples. Square points are antireflection-coated samples. The solid straight line is the least-squares fit (the same as the power law fit) to the uncoated disks. The dashed curve is the exponential law fit to uncoated samples.

strength is statistically significant at the 97% confidence level in a two-tailed $t$-test for Gaussian statistics.

### 4.2 *Dynamic Fatigue Slow Crack Growth Parameters*

Figure 3 is a graph of Eq. (4) showing 150 dynamic fatigue measurements (circles) of uncoated MS-ZnS at five stress rates spanning four orders of magnitude. The solid line is the least-squares linear fit to the 150 points. Tables 3 and 4 give observed failure stresses and the Weibull modulus for each set of 30 measurements at each stress rate.

Power law slow crack growth parameters $n$ and $A^*$ in Eq. (2) were determined from the straight line in Fig. 3. From slope $a = 0.0639$, intercept $b = 1.800$, and inert strength $\sigma_i = 114.7$ MPa (Table 2), the parameters $n = 14.65$ and $A^* = 0.0769$ m/s are found with Eqs. (5) and (6).

Best-fit exponential law crack growth parameters $v_0 = 3.02 \times 10^{-14}$ m/s and $\beta = 43.64$ $(\text{MPa}\sqrt{\text{m}})^{-1}$ for Eq. (1) were calculated by fitting the same 150 points in Fig. 3 by numerical integration with an optimized procedure to rapidly locate the optimum crack growth parameters.[8] The dashed line in Fig 3 is the exponential crack growth law fit to the 150 points calculated from $v_0$ and $\beta$ by the integration of Eq (1) at each of the five stress rates. Over the measured stress rate range, the power and exponential laws fit nearly identically.

## 5 Discussion

To the best of our knowledge, the only other dynamic fatigue measurements of MS-ZnS appeared in a 1993 report,[2] the results of which are displayed in Figs. 4 and 5 and Tables 5 and 6. Results were provided to us and reported in our 2017 paper.[3] The 1993 study used Morton Cleartran® zinc sulfide, which is made by the same general process as II-VI MS-ZnS. Five stress rates were employed with 4-point flexure specimens immersed in water. Inert strength was measured with bars immersed in liquid nitrogen to prevent slow crack growth.

Comparison of the 2021 and 1993 full data set crack growth velocities in Fig. 5 shows significant disagreement. At a stress intensity factor of $K_I = 0.25$ MPa$\sqrt{\text{m}}$, which is representative of operating conditions for an aircraft window, the 1993 exponential law predicts a crack growth rate ~200 times lower than that for the 2021 data and a widow lifetime that is ~200 times greater. We had no reason to expect that the slow crack growth rate would be substantially different in the 1993 and 2021 materials. They are both made by the same process of chemical vapor deposition

**Table 3** Dynamic fatigue and inert strength data for uncoated MS-ZnS (2021).

| | Inert strength | Dynamic fatigue | Dynamic fatigue | Dynamic fatigue | Dynamic fatigue | Dynamic fatigue |
|---|---|---|---|---|---|---|
| | $\sigma$ (MPa) | 10 MPa/s | 1 MPa/s | 0.1 MPa/s | 0.01 MPa/s | 0.001 MPa/s |
| | 51.67 | 53.71 | 43.58 | 34.54 | 27.61 | 26.88 |
| | 62.63 | 56.24 | 44.18 | 37.91 | 31.40 | 27.48 |
| | 65.28 | 56.64 | 47.21 | 40.80 | 32.62 | 28.29 |
| | 77.95 | 59.60 | 48.81 | 41.36 | 33.26 | 29.77 |
| | 86.69 | 62.30 | 48.88 | 41.88 | 36.97 | 31.56 |
| | 88.54 | 62.99 | 52.54 | 42.62 | 37.06 | 31.66 |
| | 94.02 | 63.28 | 54.88 | 42.64 | 38.84 | 32.37 |
| | 94.33 | 64.31 | 55.08 | 44.12 | 40.76 | 33.78 |
| | 98.83 | 64.61 | 55.28 | 44.94 | 40.83 | 33.90 |
| | 102.32 | 66.20 | 56.45 | 45.35 | 41.00 | 36.68 |
| | 103.64 | 66.88 | 57.07 | 45.38 | 41.91 | 37.01 |
| | 109.51 | 67.28 | 58.44 | 45.74 | 42.34 | 40.36 |
| | 111.43 | 68.39 | 60.41 | 46.62 | 44.16 | 41.97 |
| | 111.56 | 68.93 | 63.50 | 47.86 | 46.05 | 42.74 |
| | 113.89 | 69.11 | 64.82 | 49.59 | 46.48 | 43.61 |
| | 114.51 | 73.45 | 65.40 | 50.35 | 48.13 | 43.96 |
| | 116.31 | 74.66 | 66.42 | 51.26 | 51.34 | 44.32 |
| | 119.26 | 75.99 | 69.73 | 51.61 | 52.09 | 45.81 |
| | 119.62 | 76.76 | 70.30 | 62.42 | 52.56 | 46.38 |
| | 128.90 | 77.56 | 71.13 | 64.36 | 53.02 | 47.05 |
| | 131.87 | 79.74 | 73.00 | 65.00 | 53.51 | 47.52 |
| | 135.39 | 80.60 | 75.02 | 66.76 | 55.18 | 48.43 |
| | 135.52 | 83.18 | 75.59 | 67.15 | 56.33 | 49.29 |
| | 137.26 | 84.93 | 76.43 | 67.96 | 56.65 | 50.31 |
| | 137.90 | 90.59 | 79.82 | 69.38 | 58.00 | 50.89 |
| | 145.96 | 90.75 | 80.91 | 69.44 | 58.72 | 50.96 |
| | 148.06 | 94.51 | 84.80 | 70.95 | 63.24 | 51.92 |
| | 152.42 | 97.90 | 85.10 | 71.08 | 63.75 | 55.23 |
| | 155.44 | 104.63 | 87.97 | 72.73 | 67.76 | 59.62 |
| | 155.44 | 108.83 | 89.58 | 73.01 | 68.18 | 60.23 |
| Mean | 113.54 | 74.82 | 65.41 | 54.16 | 47.99 | 42.33 |
| Std. dev. | 27.92 | 14.40 | 13.49 | 12.47 | 11.00 | 9.49 |
| Weibull $m$ | 4.68 | 5.14 | 5.25 | 4.69 | 4.72 | 4.91 |

**Table 4** Dynamic fatigue and inert strength data for coated MS-ZnS (2021).

| | Inert strength | Dynamic fatigue | Dynamic fatigue |
|---|---|---|---|
| | $\sigma$ (MPa) | 10 MPa/s | 0.01 MPa/s |
| | 45.49 | 41.64 | 29.45 |
| | 57.88 | 44.90 | 32.01 |
| | 68.22 | 47.23 | 32.84 |
| | 76.92 | 47.63 | 33.44 |
| | 77.45 | 51.64 | 34.06 |
| | 83.75 | 52.15 | 37.97 |
| | 86.60 | 53.45 | 38.37 |
| | 88.42 | 55.10 | 39.44 |
| | 88.83 | 56.37 | 40.24 |
| | 90.99 | 57.45 | 42.01 |
| | 91.72 | 57.60 | 42.93 |
| | 91.80 | 61.73 | 46.80 |
| | 93.81 | 62.21 | 46.85 |
| | 95.08 | 62.82 | 47.21 |
| | 96.22 | 64.68 | 49.79 |
| | 99.29 | 66.41 | 49.82 |
| | 100.43 | 66.65 | 49.96 |
| | 101.93 | 68.28 | 50.28 |
| | 103.32 | 68.92 | 50.42 |
| | 104.92 | 73.01 | 51.33 |
| | 106.79 | 73.34 | 52.65 |
| | 108.34 | 74.02 | 56.67 |
| | 117.10 | 83.87 | 57.28 |
| | 120.01 | 85.91 | 59.12 |
| | 122.68 | 89.85 | 59.76 |
| | 124.60 | 90.48 | 64.48 |
| | 124.74 | 92.52 | 64.56 |
| | 126.04 | 93.23 | 66.74 |
| | 131.41 | 98.50 | 74.67 |
| | 134.90 | 99.53 | 75.05 |
| Mean | 98.66 | 68.04 | 49.21 |
| Std. dev. | 21.34 | 16.87 | 12.32 |
| Weibull $m$ | 5.25 | 4.24 | 4.17 |

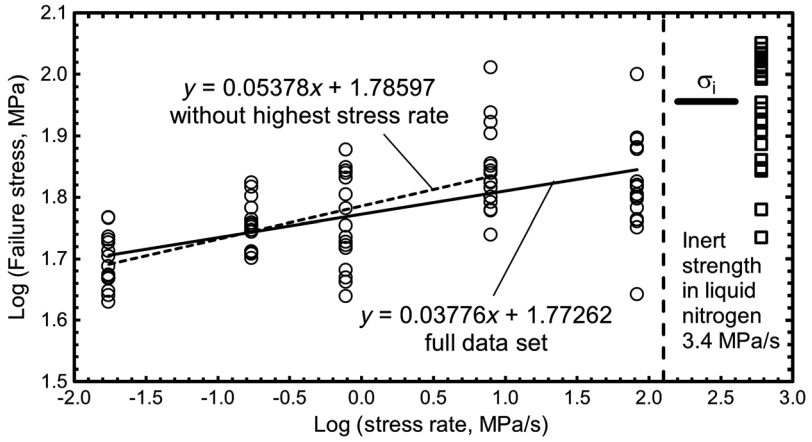


**Fig. 4** Dynamic fatigue measurement of Morton Cleartran® zinc sulfide 4-point flexure bars immersed in water at 21°C.[2] The least-squares slope and intercept are fit to all points in either four of the stress rates or all five stress rates. Inert strength measured in liquid nitrogen was $\sigma_i =$ 90.4 MPa (50% probability of failure on the Weibull curve). The study employed ASTM C1161[25] type C bars with dimensions of 6 mm × 8 mm × (90 mm or 100 mm) with 40 mm load span and 80 mm support span.

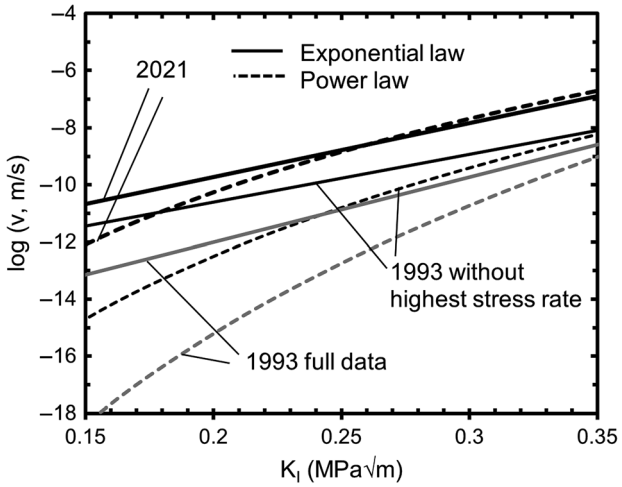


**Fig. 5** Comparison of 2021 and 1993 ZnS slow crack growth velocities.

followed by hot isostatic pressing while wrapped in platinum foil. Their optical and elastic properties and fracture toughness are equal within measurement uncertainty.

This disagreement in the slow crack growth rate led us to examine the 1993 data more carefully. In Fig. 4 the average failure stress at the highest stress rate of 82.7 MPa/s is 67 MPa. The average failure stress at the second-highest stress rate of 7.9 MPa/s is 71 MPa. The strength at higher stress rates should be greater than the strength at lower stress rates because there is 1/9 as much time for slow crack growth to occur at the higher stress rate. We speculate that the highest-stress-rate data might be invalid, perhaps because the test machine could not implement the highest stress rate or measure stress accurately at the highest stress rate.

Figure 4 shows an alternate interpretation of the 1993 data in which the highest stress rate is discarded. The dynamic fatigue fit shown by the dashed line has a greater slope than the fit to the full data set. The exponential law derived by omitting the highest-stress-rate data is shown in Fig. 5 and is closer to the 2021 exponential law. At the service stress intensity factor $K_I =$ 0.25 MPa$\sqrt{\text{m}}$, the 1993 and 2021 window lifetime predictions differ from each other by a factor of 10 rather than a factor of 200 predicted by the full 1993 data set.

**Table 5** Dynamic fatigue and inert strength data for Cleartran® zinc sulfide (1993).

| | Inert strength | Dynamic fatigue | Dynamic fatigue | Dynamic fatigue | Dynamic fatigue | Dynamic fatigue |
|---|---|---|---|---|---|---|
| | $\sigma$ (MPa) | 82.7 MPa/s | 7.93 MPa/s | 0.779 MPa/s | 0.172 MPa/s | 0.0174 MPa/s |
| | 54.33 | 43.8 | 54.8 | 43.5 | 50.2 | 42.6 |
| | 60.28 | 56.3 | 59.9 | 45.9 | 51.0 | 43.7 |
| | 69.67 | 57.6 | 60.2 | 46.7 | 51.2 | 44.4 |
| | 70.51 | 58.0 | 61.9 | 48.0 | 51.5 | 46.5 |
| | 72.61 | 60.6 | 63.1 | 52.1 | 55.4 | 46.6 |
| | 77.02 | 62.7 | 65.3 | 52.7 | 55.8 | 46.7 |
| | 81.07 | 63.1 | 66.6 | 53.4 | 56.4 | 47.0 |
| | 83.51 | 63.7 | 66.8 | 54.3 | 56.8 | 47.2 |
| | 84.48 | 65.6 | 69.0 | 56.7 | 56.9 | 48.7 |
| | 88.12 | 66.0 | 69.6 | 60.5 | 57.3 | 50.6 |
| | 90.13 | 66.8 | 70.9 | 63.7 | 58.0 | 51.6 |
| | 98.51 | 75.5 | 71.5 | 67.8 | 60.6 | 53.3 |
| | 99.37 | 76.1 | 80.1 | 69.0 | 63.3 | 53.8 |
| | 101.32 | 78.4 | 83.6 | 69.6 | 65.6 | 54.4 |
| | 103.09 | 78.8 | 86.6 | 70.5 | 66.6 | 58.4 |
| | 104.93 | 100.0 | 102.5 | 75.3 | | 58.5 |
| | 106.77 | | | | | |
| | 108.35 | | | | | |
| | 110.15 | | | | | |
| | 112.62 | | | | | |
| Mean | 88.84 | 67.06 | 70.78 | 58.11 | 57.11 | 49.63 |
| Std. dev. | 17.42 | 12.71 | 12.11 | 10.11 | 5.14 | 4.95 |

**Table 6** Slow crack growth parameters derived from dynamic fatigue studies.[a]

| | Dynamic fatigue | | Power law | | Exponential law | |
|---|---|---|---|---|---|---|
| Data set | Slope ($a$) | Intercept ($b$) | $A^*$ (m/s) | $n$ | $v_o$ (m/s) | $\beta$ |
| 2021 uncoated disks | 0.06389 | 1.8000 | 0.00769 | 14.65 | 3.02E-14 | 43.64 |
| 1993 full data set 4-pt flexure | 0.03776 | 1.7726 | 0.09038 | 25.49 | 2.75E-17 | 52.42 |
| 1993 omit highest stress rate | 0.05378 | 1.7860 | 0.00192 | 17.59 | 1.11E-14 | 38.63 |

[a]$K_{Ic} = 0.72$ MPa$\sqrt{\text{m}}$, $Y = 2/\sqrt{\pi}$.

## 6 Summary

Mechanical properties necessary to design a sensor window were measured on multispectral zinc sulfide. Inert strength was characterized by Weibull parameters describing the strength distribution. Dynamic fatigue data were fit using both power and exponential crack growth laws. Results were compared with measurements made in 1993 on Cleartran® ZnS, which is made in essentially the same manner as MS-ZnS. The observed slow crack growth velocity in the present work is one or two orders of magnitude greater than previously reported.

## Acknowledgments

The authors declare no conflicts of interest.

## References

1. D. C. Harris, "Development of hot-pressed and chemical-vapor-deposited zinc sulfide and zinc selenide in the United States for optical windows," *Proc. SPIE* **6545**, 654502 (2007).
2. University of Dayton Research Institute, *Characterization of Cleartran ZnS*, Final report for subcontract 417424, Dayton, Ohio (1993).
3. L. R. Cambrea et al., "Slow crack growth study of polycrystalline alumina and multispectral zinc sulfide," *Proc. SPIE* **10179**, 101790A (2017).
4. S. M. Wiederhorn, "Influence of water vapor on crack propagation in soda-lime glass," *J. Am. Ceram. Soc.* **50**(8), 407–414 (1967).
5. S. M. Wiederhorn, "Moisture assisted crack growth in ceramics," *Int. J. Fract.* **4**(2), 171–177 (1968).
6. ASTM C1368, *Standard Test Method for Determination of Slow Crack Growth Parameters of Advanced Ceramics by Constant Stress-Rate Flexural Testing at Ambient Temperature*, ASTM International, West Conshohocken, Pennsylvania (2018).
7. ASTM C1465, *Standard Test Method for Determination of Slow Crack Growth Parameters of Advanced Ceramics by Constant Stress-Rate Flexural Testing at Elevated Temperatures*, ASTM International, West Conshohocken, Pennsylvania (2019).
8. C. M. Ryan, K. R. Johnson, and D. C. Harris, "Deriving exponential law slow crack growth parameters from dynamic fatigue of indented or as-polished window coupons," *Opt. Eng.* **61** (2022).
9. "NASA STD 5018 approved 12 Aug 2011 revalidated 27 Nov 2017," https://standards.nasa.gov/standard/nasa/nasa-std-5018.
10. S. R. Choi and J. P. Gyekenyesi, "Fatigue strength as a function of preloading in dynamic fatigue testing of glass and ceramics," *J. Eng. Gas Turbines Power* **119**(3), 493–499 (1997).
11. S. R. Choi and J. A. Salem, "Preloading technique in dynamic fatigue testing of glass and ceramics with an indentation flaw system," *J. Am. Ceram. Soc.* **79**(5) 1228–1232 (1996).
12. S. R. Choi and J. P. Gyekenyesi, *Results of Mechanical Testing for Pyroceram Glass Ceramic*, NASA/TM-2003-212487, National Aeronautics & Space Administration, Glenn Research Center, Cleveland, Ohio (2003).
13. J. E. Ritter, N. Bandyopadhyay, and K. Jakus, "Statistical reproducibility of the dynamic and static fatigue experiments," *Am. Ceram. Soc. Bull.* **60**(8), 798–806 (1981).
14. D. K. Shetty et al., "Biaxial flexure test for ceramics," *Am. Ceram. Soc. Bull.* **59**(12), 1193–1197 (1980).
15. ASTM C1421, *Standard Test Methods for Determination of Fracture Toughness of Advanced Ceramics at Ambient Temperature*, ASTM International, West Conshohocken, Pennsylvania (2019).
16. J. Kübler, *Fracture Toughness of Ceramics using the SEVNB Method: Round Robin*, VAMAS Report No. 37, EMPA, Swiss Federal Laboratories for Materials Testing & Research, Dübendorf, Switzerland (1999).
17. S. R. Choi and J. P. Gyekenyesi, *Assessments of Fracture Toughness of Monolithic Ceramics - SEPB Versus SEVNB Methods*, NASA/TM-2006-214090, National Aeronautics & Space Administration, Glenn Research Center, Cleveland, Ohio (2006).

18. ASTM C1259, *Standard Test Method for Dynamic Young's Modulus, Shear Modulus, and Poisson's Ratio for Advanced Ceramics by Impulse Excitation of Vibration*, ASTM International, West Conshohocken, Pennsylvania (2021).
19. ASTM C1327, *Standard Test Method for Vickers Indentation Hardness of Advanced Ceramics*, ASTM International, West Conshohocken, Pennsylvania (2019).
20. J. A. Salem and M. G. Jenkins, "Applying ASTM C1421 to glasses and optical ceramics," in *Ceram. and Eng. Proc. (2018). Proc. 42nd Int. Conf. Adv. Ceram. and Compos.*, Daytona Beach, Florida (2017).
21. C. Klein and C. B. Willingham, "Elastic properties of chemically vapor-deposited ZnS and ZnSe," in *Basic Properties of Optical Materials*, NBS Special Publication 697, A. Feldman, Ed., pp. 137–140, U. S. National Bureau of Standards, Gaithersburg, Maryland (1985).
22. D. C. Harris et al., "Thermal, structural, and optical properties of Cleartran® multispectral zinc sulfide," *Opt. Eng.* **47**(11), 114001 (2008).
23. ASTM C1239, *Standard Practice for Reporting Uniaxial Strength Data and Estimating Weibull Distribution Parameters for Advanced Ceramics*, ASTM International, West Conshohocken, Pennsylvania (2018).
24. ASTM C1499, *Standard Test Method for Monotonic Equibiaxial Flexure Strength of Advanced Ceramics at Ambient Temperature*, ASTM International, West Conshohocken, Pennsylvania (2019).
25. ASTM C1161, *Standard Test Method for Flexure Strength of Advanced Ceramics at Ambient Temperature*, ASTM International, West Conshohocken, Pennsylvania (2018).

**Colin M. Ryan** is a materials engineer at the Naval Air Warfare Center Weapons Division, China Lake, California. He received his BS degree in ceramic engineering from Missouri University of Science and Technology and his MS degree in materials science and engineering from Clemson University. His areas of focus include glass and ceramic electromagnetic window materials.

**Daniel C. Harris** is a senior scientist and esteemed fellow at the Naval Air Warfare Center Weapons Division, China Lake, California, where he is responsible for infrared window materials research and development programs. He has chemistry degrees from Massachusetts Institute of Technology (S.B. 1968) and California Institute of Technology (PhD 1973). He is the author of the monograph *Materials for Infrared Windows and Domes* (SPIE Press 1999) and a series of textbooks on analytical chemistry.

**Jared C. Wright** received his master's degree in materials engineering from Purdue University in 2010. He worked in the Ceramics and Transparent Materials Branch at the US Army Research Laboratory from 2011 to 2015. In 2015, he moved to the Naval Air Warfare Center Aircraft Division, where he supports naval aviation through system acquisition, technology transfer, and materials research.

**Sung R. Choi** is a science and technology lead in materials engineering and an associate fellow at the Naval Air Warfare Center Aircraft Division. He is responsible for advanced materials systems in their applications to aero-propulsion components. He received his MS degree and PhD in mechanical engineering from the University of Washington and the University of Massachusetts—Amherst, respectively. He has written more than 220 technical articles on brittle and propulsion materials and is a fellow of ASME.

**Ashlynn M. Stanley:** Biography is not available.